TeV Gamma-Ray Observations and the Origin of Cosmic Rays III.

H.J. Völk
Max-Planck-Institut für Kernphysik, D-69029 Heidelberg, Germany

Abstract

The present final part of a triad of plenary talks on the results of high energy gamma-ray astronomy and the origin of Cosmic Rays is primarily devoted to the physics interpretation. I will start with the stereoscopic method of operating several imaging atmospheric Cherenkov telescopes in coincidence as pioneered by HEGRA, and a summary description of the results obtained. Then I will turn to the search for gamma rays from Supernova Remnants over the last decade and argue that only the quantitative comparison of observations with a consistent theory of particle acceleration can lead to a generally acceptable picture of Cosmic Ray origin. The elements of this theory are outlined. It is subsequently used to model SN 1006 and Cassiopeia A, the two sources that until now could be investigated to the required detail. The analysis shows for the first time that emission spectra and morphological detail are in agreement with the concept that these two distinctly different objects are representative members of a suspected Supernova source population in the Galaxy. The continuing study of this population is an essential part of the program of the major new gamma-ray instruments.

1. The HEGRA Stereoscopic System

Representing also the HEGRA experiment in this overview I want to emphasize first the significance of the stereoscopic method in ground-based γ-ray astronomy. This observation technique positions several telescopes in the Cherenkov light pool on the ground so that the same gamma-ray shower in the atmosphere is observed from different positions, in a manner analogous to the practice of a land surveyor (Fig. 1). The reconstruction of the γ-ray direction is achieved on a purely geometrical basis by combining the different shower images into a single focal plane detector ("camera"). The shower impact point on the ground is reconstructed similarly from the images in the spatially seperated telescopes. An immediate result is increased angular resolution and a higher energy resolution. At the same time it is possible to strongly improve background rejection, in particular against local muons from unrecognized showers in the distant atmosphere. The energy threshold for such a system is therefore lower than for each of the individual telescopes seperately.

pp. 1–?? ©2003 by Universal Academy Press, Inc.

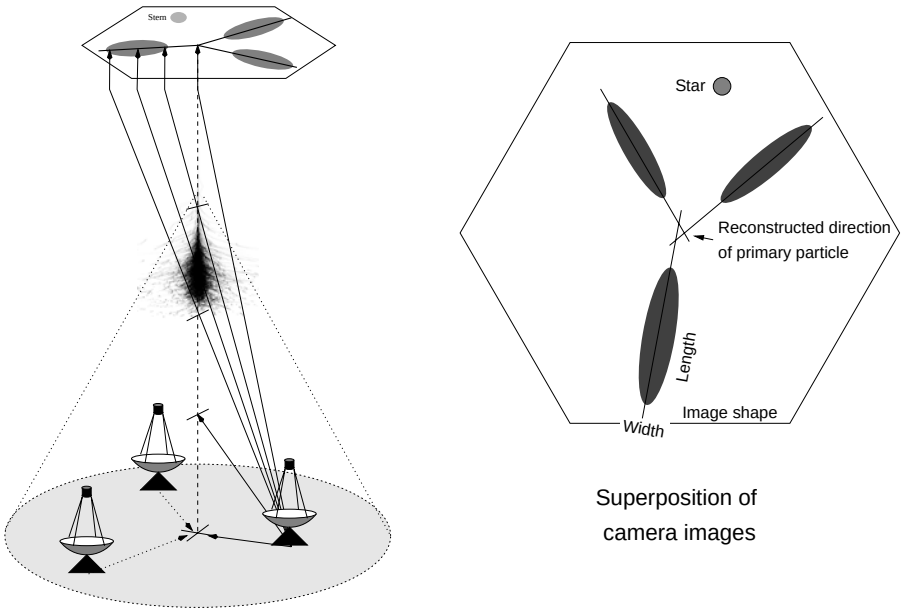

Fig. 1. Schematic of stereoscopic γ-ray observations. The Cherenkov light of the shower electrons illuminates a cone whose basis on the ground has a radius of about 120 m. Pointing telescopes inside the Cherenkov cone see the shower under different angles (left panel). The elongated shower images in the focal plane (with a length exceeding their width) point towards the primary γ-ray direction. Bringing the various images into a single camera allows a geometric reconstruction of the γ-ray direction. An analogous image extrapolation from the seperated telescopes yields the shower impact point on the ground (right panel). Courtesy G. Pühlhofer.

The stereoscopic array of the HEGRA experiment on La Palma which was finally dismantled in late 2002 has been combining five relatively small telescopes of 3.3 m effective diameter (8.5m^2 mirror area) each. Using the technique described above it was able to detect and thereby to confirm all the Northern Hemisphere sources originally detected by the (single) 10 m (75m^2 mirror area) Whipple telescope in Arizona. In addition, the HEGRA system detected a number of very weak sources like the first unidentified TeV source TeV J2032+4130 in the Galaxy, the first Northern Hemisphere Supernova Remnant Cassiopeia A (Cas A; Fig.2), and the first radio galaxy in the TeV range: M87 in the center of the Virgo cluster. Consistent with their fluxes of merely several percent of the Crab Nebula, the three new sources could not yet be confirmed by other instruments.

I shall not enter into a discussion about the overall observational results of TeV γ-ray astronomy which the previous speakers, T.C. Weekes and T. Kifune, have already presented so ably for the Extragalactic and the Galactic sources.

My assignment here is rather to interprete these results with regard to the origin of Cosmic Rays (CRs). More specifically I shall ask the question, whether and to which extent the TeV-detection of Supernova Remnants (SNRs) in our Galaxy has solved this problem which has eluded physicists for more than ninety years, since the discovery of Victor Hess in 1912.

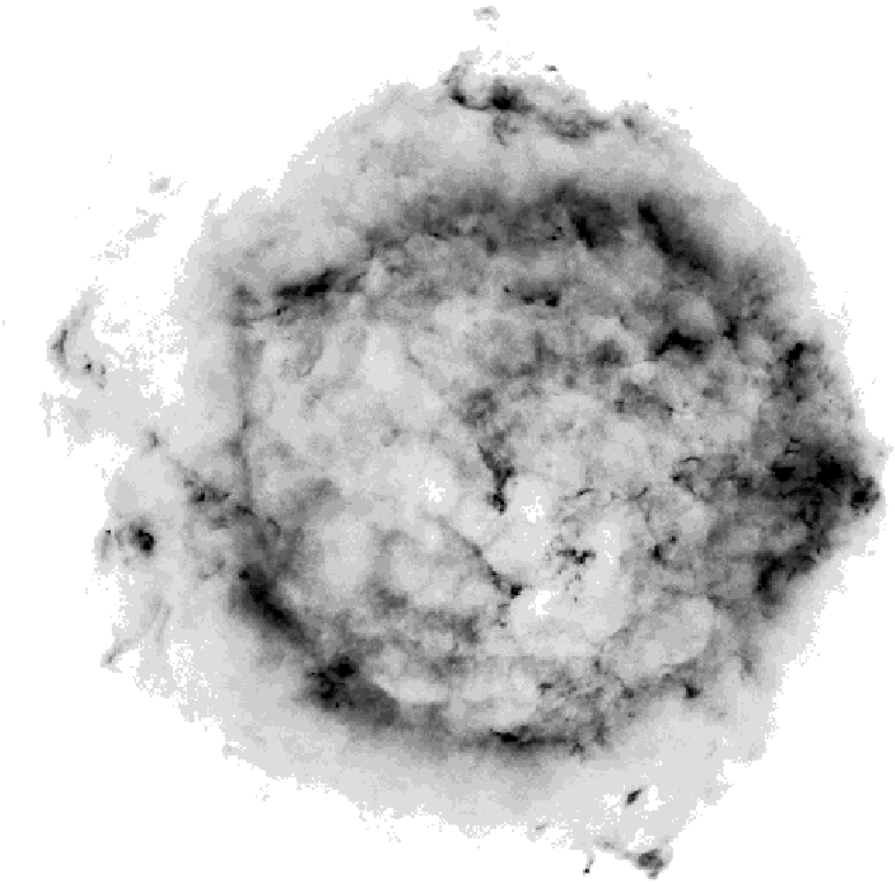

Fig. 2. Cas A observed in 6 cm radio wavelengths with the VLA (R.J. Tuffs, 1986). The bright ring of emission is interpreted as the result of a compressed circumstellar wind shell [51], with strongly amplified magnetic field [53].

2. Test of the Supernova Remnant origin of Cosmic Rays

Following the hypothesis of Baade and Zwicky from 1934, that Supernova explosions might be the ultimate sources of the CRs [1], the idea has been entertained in various forms. Indeed as time progressed it became more and more clear that

there are not many viable alternatives from an energetics point of view. And it has slowly become a common belief that the shocks in the circumstellar medium, produced by the violently expanding SNRs, should accelerate the CRs in the Galaxy up to about the knee in the all-particle energy spectrum at several 10^{15} eV.

From an experimental point of view it is obvious that any real test can only come through characteristic radiation signatures from the dominant nuclear particles in individual objects, at comparable energies. The most direct way to achieve this test is the detection of gamma-rays at TeV energies.

2.1. Practical beginning of the source search

This effort began in earnest about ten years ago when time-dependent nonlinear acceleration models in SNRs, still in a hydrodynamic approximation also for the CR component, were used to calculate the expected γ-ray emission. The models had to assume the form of the energetic particle spectrum, consistent with the calculated time evolution of the total energy in CRs, and in detail they turned out to be sensitive to the assumed injection rates at suprathermal energies [2,3]. While these dynamic models concentrated on the nuclear γ-rays from π^0-decay following inelastic collisions with nuclei from the thermal gas, there was also a class of kinematic models by e.g. Naito & Takahara [4] and Gaisser et al. [5] who rather assumed distributions of accelerated nuclei and energetic electrons but then concentrated on the various radiation processes from these particle populations and their relative importance. Subsequently γ-ray emission models were developed from kinetic theory by Berezhko & Völk [6,7]. They involved numerical solutions of the full time-dependent, nonlinear CR transport equation in spherical symmetry which had been first obtained by Berezhko et al. [8,9]. Based on stationary plane wave solutions of the same transport equations with a Monte Carlo code [10], Baring et al. [11] also estimated the time-dependent γ-ray emission.

The conclusions from this theoretical work were cautiously optimistic: nuclear TeV γ-rays from bright nearby objects should be marginally detectable by existing ground-based instruments.

2.2. Early observational attempts

The first specific γ-ray observations were made in the early nineties. However the initial results were rather inconclusive. Esposito et al. [12] had observed several shell-type SNRs, notably G78.2+2.1 (γ-Cygni) and IC443, with the EGRET instrument on CGRO at γ-ray energies below 1 GeV. Subsequent TeV observations by the Whipple [13] and HEGRA [14] groups yielded only upper limits. For γ-Cygni and IC 443 these upper limits were below the power-law extrapolations of the EGRET spectra and, like the Whipple upper limit for Tycho's SNR, they tended also to lie below the theoretical estimates [3] for the π^0-decay γ-ray flux. In contrast a first TeV-detection was reported for the Southern Hemisphere rem-

nant of SN 1006 by the CANGAROO collaboration [15]. The flux value given significantly exceeded the expected π^0-decay flux [16].

The failure to detect TeV emission from the EGRET sources could be understood if in reality a straight extrapolation of the power law spectrum from EGRET energies to the TeV range was not required. The expected emissions would then come from different objects. Alternatively the remnant could be "old" in an evolutionary sense, having lost many of its very high energy particles already (see the section on Cas A). Such doubts were substantiated by Brazier et al. [17] who rather found a Pulsar in the EGRET 95 % error box for γ-Cygni, and Pulsars are generally assumed to exhibit a cutoff in the emission spectrum at some tens of GeV. In IC443 Keohane et al. [18] found only two regions with hard X-ray emission from high energy ($\sim$ 10 TeV) electrons, certainly not over most of the radio shell. An association between the hard X-ray sources and the EGRET source can not be firmly established either (see [19], which also contains a summary of the recent X-ray results). More generally speaking, no unambiguous EGRET detection of a shell-type SNR exists. This is one of the questions which the GLAST mission will have to resolve.

2.3. SNR detections in nonthermal hard X-rays and TeV γ-rays

In the mid-nineties SN 1006 was detected in hard X-rays [20,21] and much of this emission was attributed to synchrotron radiation of electrons with energies of tens of TeV [20,22], see Fig. 3a. Subsequently also several other shell-type remnants where shown to have power law tails in their emission, notably SNR RX J1713.7-3946 in the Southern Hemisphere [24,25] and Cas A [26].

The question was then, whether the energetic electrons would not also be visible in TeV γ-rays through their Inverse Compton (IC) scattering on ambient low energy photons, primarily from the Cosmic Microwave Background (CMB) [27,28]. In 1998 the CANGAROO collaboration published its detection of SN 1006 [15] mentioned earlier, and interpreted it in terms of IC emission. A subsequent TeV detection of SNR RX J1713.7-3946 with the same telescope [29] was given an analogous interpretation. The only critical discussion at the time was published by Atoyan and Aharonian [30].

The prevalent opinion that there was no need for nuclear CRs to explain the TeV γ-ray emission from SNRs gave room to doubts as to the existence of any significant quantities of CR nuclei in shell-type SNRs at all [31]. However this pessimistic turn was provoked by phenomenological arguments not by theory, as all the arguments before. Again on a phenomenological basis, the CANGAROO collaboration on the other hand reversed its view regarding SNR RX J1713.7-3946 by presenting new arguments which now favored a hadronic γ-ray origin [32] (see also [25] above). This led to a controversial discussion, where several groups [33,34] gave empirical counterarguments which questioned the new interpretation.

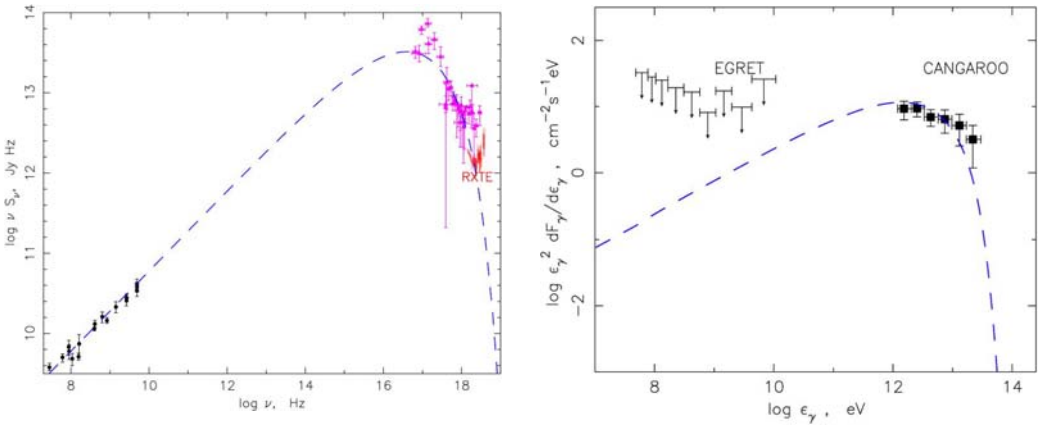

Fig. 3. a. Synchrotron and γ-ray emission from SN 1006. Radio data are from [22], X-ray data are from [21] and [23]. Approximately a power law plus cutoff (*dashed curve*) for the electron distribution in a weak field of several μG has been used in a phenomenological fit of the data. b. The same electron spectra are used for an IC fit to the differential γ-ray energy flux data reported in [36]. Also the EGRET upper limits are shown.

Unfortunately SNR RX J1713.7-3946 is a complex source which may either be the result of the thermonuclear explosion/deflagration of an accreting White Dwarf (SN Type Ia) that ejects a Chandrasekhar mass, or of the core collapse of a massive star. The distance uncertainty ranges from 1 to 6 kpc [24, 25]. The remnant is situated in a complex interstellar environment (e.g. [35]) and is far less well studied than SN 1006, for example. Therefore the debate remains quite inconclusive at present. SN 1006 is a much clearer case. It is a SN type Ia, with excellent radio and X-ray observations and extensive morphological studies. Fig. 3b shows the latest published γ-ray results [36], with an IC fit for the spectrum.

Our own conclusion was that phenomenological considerations are important but that they will not give a convincing answer to the question of the acceleration of CR nuclei in SNRs as reasonable as they may appear individually, one by one. There is a need for quantitative comparison of the observations with a consistent theory, as in other areas of physics. Contradictory interpretations of the observations can be excluded only if such a detailed picture is available.

3. Theory of diffusive shock acceleration as applied to SNRs

Let me summarize such a theory in three cartoons. Obviously they are only meant to illustrate the essential physics; the real description is given by the equations which I shall only write down to hint at the mathematical aspects. Much of the theory is reviewed in e.g. [37,38,39,40,41].

The left cartoon of Fig. 4 shows the spatial dependence in a plane shock, propa-

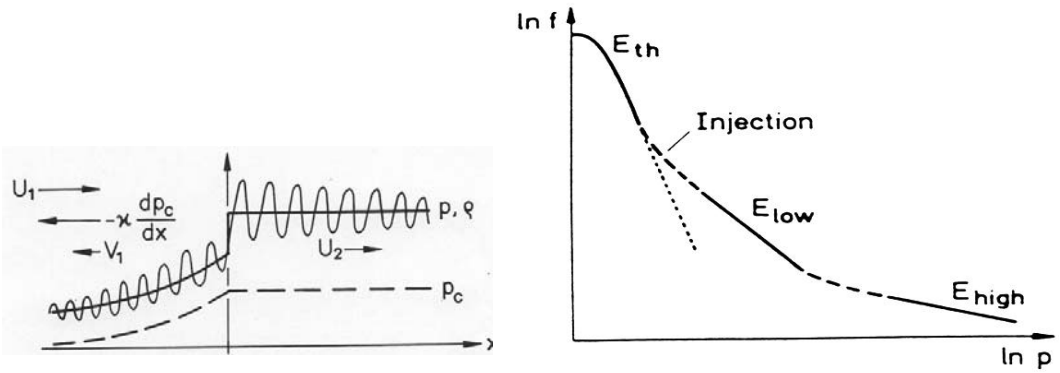

Fig. 4. Spatial dependence of flow velocity U_i, gas pressure (denoted here by p), mass density ρ, and CR pressure p_c, in the regions upstream (i=1) and downstream (i=2) of a plane shock, as a function of the space coordinate x in the shock frame of reference. The wavy line indicates the growing amplitude of the scattering magnetic fluctuations of the Alfvénic wave field which is excited by the diffusive CR current $-\kappa dp_c/dx$ into the upstream precursor region and compressed in the subshock at $x = 0$. V_1 is the wave phase velocity vector in the upstream fluid frame. Particles gain energy by repeated scatterings across the shock (left panel). The right panel shows the momentum dependence of the downstream particle distribution. The three regions joined by dashed lines correspond to the thermal plasma, characterized by the thermal energy (E_{th}) and extrapolated by a dotted curve, the low-energy nonthermal particles (E_{low}), and the high-energy particles (E_{high}), respectively.

gating parallel to the magnetic field. The nonlinear backreaction of the accelerated particles on the dynamics of the thermal gas through their pressure gradient creates a smooth precursor, followed by a sharp subshock, where the fluid quantities of the thermal gas jump discontinuously. The CR pressure

$$p_c = \frac{4\pi c}{3} \int_{p_{inj}}^{\infty} dp \frac{p^4 f(x,p,t)}{\sqrt{p^2 + m^2 c^2}} \tag{1}$$

is given in terms of the isotropic part of the particle distribution function $f(x, p, t)$, averaged over the magnetic fluctuations; the quantities p and m denote the magnitude of particle momentum and its mass. In the downstream distribution (right panel) CRs are characterized by momenta above the region of injection where downstream particles can outrun the shock along the magnetic field. The nonthermal spectrum starts with a steep power law distribution, characterized by diffusive acceleration at the subshock only. High energy particles "see" the entire compression as a discontinuity and have therefore a harder spectrum that begins in the region where protons become ultrarelativistic [9].

Strong shocks with Alfvénic Mach numbers $M_a = U_1/V_1 \gg 1$ typically inject so many suprathermal nuclear particles into the acceleration process that the acceleration is efficient, $p_c \sim \rho_1 U_1^2$, and that nonlinear backreaction leads to a

strong precursor. In SNRs M_a is of order 10^3 at very early times, and for SN 1006 it is still as large as 150 at the present epoch. Thus the total compression ratio $r_{tot} > 4$, whereas the subshock compression ratio $r_{sub} < 4$. Only part of the overall energy dissipation goes into thermal energy at the subshock, the rest is given to the energetic particles and to the growing waves.

The most difficult aspect of particle acceleration is the magnetic field and its fluctuations, because this field is what the energetic particles interact with directly. And the field is not simply given externally, but is rather excited by the particles themselves as another part of the nonlinearity of the process.

The selfconsistent wave production by the accelerated particles themselves can only be estimated rather approximately. A simple-minded quasilinear calculation [42] for efficient acceleration leads to an extremely large wave field $\delta B/B \gg 1$, where δB is the total rms wave amplitude and B is the assumed mean magnetic field strength. This conclusion has been shown to hold also differentially for the wave energy per unit logarithmic bandwidth in wave number in relation to the resonant energetic particle pressure $P_c(p) = 4\pi c/3\ p^4 f(x,p,t)/\sqrt{p^2+m^2c^2}$ per logarithmic interval in p [41].

However, such a result defeats the original assumption $\delta B/B \ll 1$ of perturbation theory, on which the derivation of the result is predicated (I will loosely continue to use the term δB for both the differential and the integral wave amplitude). The question is then how to deal with this outrageous situation. In fact, theory has no precise solution at the moment. Apart from wave damping, the simplest and physically most plausible conclusion is that the strong wave production amplifies the mean field to an effective field $B_{eff} \gg B_0$ [38], with $\delta B/B_{eff} \sim 1$. In this limit the scattering mean free path λ_{mfp} reaches its minimum value $r_{gyro}(p)$, where r_{gyro} is the particle gyro radius in the field B_{eff}. This is the so-called Bohm limit in the effective field and implies an isotropic diffusion particle coefficient $\kappa(p, B_{eff}) = v r_g(p)/3$. Field amplification has recently been successfully calculated in a simplified nonlinear model of wave turbulence by Lucek & Bell [43] and Bell & Lucek [44]. The result is the Bohm limit. As a scaling relation for strong shocks it is already suggested by perturbation theory.

Finally strong wave production has also profound consequences for the rate and the geometry of ion injection (third cartoon of Fig. 5a): where on the shock surface injection can occur in the first place – in an approximately spherical shock propagating in an inhomogeneous external magnetic field this is only possible in the "polar" regions – it occurs only at those field lines that are instantaneously quasi-parallel to the subshock normal direction. On all other field lines injection is suppressed until the field changes back to quasi-parallel. This has the consequence that the ion injection rate (the fraction of the incoming flux of thermal particles that can be accelerated) is reduced by about two orders of magnitude compared to that in a laminar magnetic field. The precise numerical value of the

reduction factor depends on the wave spectrum. For a uniform ambient field the systematic reduction of injection will lead to dipolar asymetries in the nonthermal morphology and requires a renormalization of the overall particle production rate, as calculated in spherical symmetry, by a factor $f_{re} < 1$ [45].

The resulting theory, applied to the dynamics of a SNR and assuming spherical symmetry, looks as follows:

CR transport and acceleration at shocks is described by a Fokker-Planck equation for the isotropic part of the mean particle distribution $f_i(p, r, t)$ for ions (p) and electrons (e), respectively:

$$\frac{\partial f_{\rm i}}{\partial t} - \nabla\kappa\nabla f_{\rm i} + \vec{U}\nabla f_{\rm i} - \frac{\nabla\vec{U}}{3}p\frac{\partial f_{\rm i}}{\partial p} + \frac{1}{p^2}\frac{\partial}{\partial p}\left(\frac{p^3}{\tau_{\rm i}}f_{\rm i}\right) = Q_i, \tag{2}$$

where the coefficients in the transport eqs. are given by the mean mass velocity $\vec{U}(r, t)$ and its divergence, as determined from the hydrodynamic eqs., and by a common diffusion coefficient $\kappa(p, B_{eff})$ as a result of scattering by the fluctuating magnetic field. Q_i denotes the injection rate, and $\tau_{\rm i}$ is the loss time, taken to be zero for ions and equal to the synchrotron loss time for electrons.

The hydrodynamics of the thermal plasma, even if we consider it as an ideal fluid, is in turn nonlinearly coupled with the energetic particles through the CR pressure gradient dp_c/dx, defined above, as well as wave dissipation, see e.g. [7]:

$$\frac{\partial\rho}{\partial t} + \nabla(\rho\vec{U}) = 0, \tag{3}$$

$$\rho\frac{\partial\vec{U}}{\partial t} + \rho(\vec{U}\nabla)\vec{U} = -\nabla(p_c + p_g), \tag{4}$$

$$\frac{\partial p_g}{\partial t} + (\vec{U}\nabla)p_g + \gamma_g(\nabla\vec{U})p_g = \alpha_a(1-\gamma_g)c_a\nabla p_c, \tag{5}$$

where ρ, $\gamma_g = 5/3$ and p_g denote the mass density, gas specific heat ratio and gas pressure, respectively. Gas heating due to Alfvén wave dissipation in the upstream region is described by the parameter $\alpha_a \leq 1$.

Already in this lowest approximation the theory involves a time-dependent nonlinear system of coupled partial integro-differential equations.

In principle the theory is quite general and can be used to describe any ionized system in which matter dominates and thermal gas motions are nonrelativistic. The above application to point explosions like SNRs is the simplest one from an analytical point of view. Astrophysically speaking it is nevertheless fundamental. In this case the theory contains only two "parameters" that are not very well calculable quantitatively: B_{eff}, and the ion injection rate Q_p. They are strongly related through the nonlinear development of wave production discussed

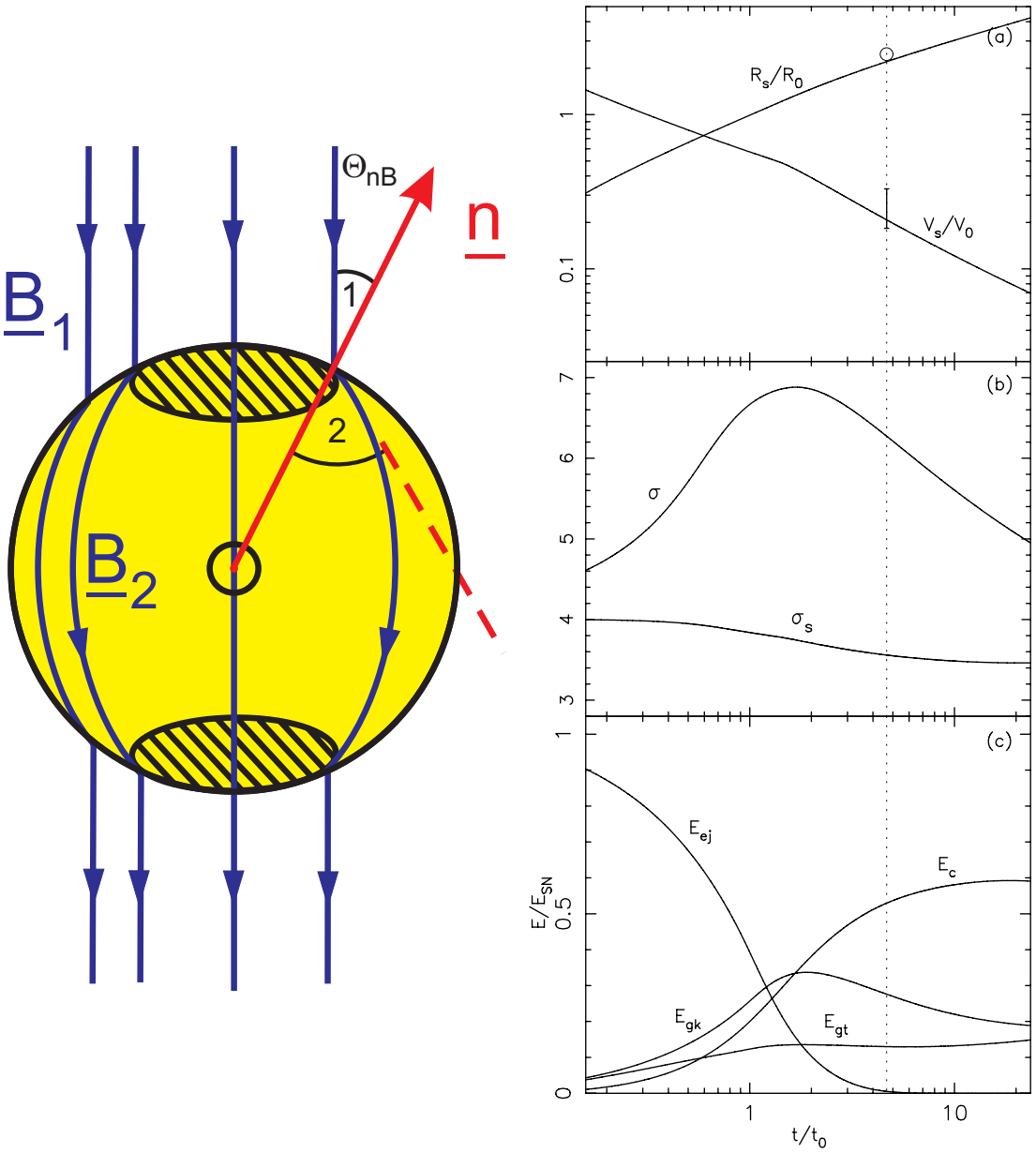

Fig. 5. Left panel: Ion injection into diffusive shock acceleration. Only for Θ_{nB_2} sufficiently smaller than 90° suprathermal ions can escape upstream along the magnetic field $\underline{B}$. In a spherical SNR in a uniform field $\underline{B}_1$, injection, strong wave production and acceleration is only possible in the *hatched* polar regions. Therefore hadronic γ-ray emission is dipolar and the same is true for the synchrotron emission as a result of field amplification. The right panel contains the temporal evolution of the overall dynamics for SN 1006 [46]. For external density $n = 0.3\ cm^{-3}$ the shock radius R_s and velocity V_s are exhibited together with the observed values. Total, σ, and subshock, σ_s, compression ratios are given in the middle panel. The quantities E_{SN}, E_{ej}, E_{gk}, E_{gt} and E_c denote the total SNR mechanical, ejected, gas kinetic, gas thermal, and un-renormalized CR energy contents, respectively.

above. It is therefore plausible to use an experimental/observational input for these parameters in order to be free from uncertain theoretical approximations.

How do we achieve this observational input for SNRs? The natural solution is given in terms of the electron component and the corresponding sychrotron observations [46]. The electrons are parasitically accelerated together with the nuclear particles which generate the scattering wave field through their dominant mass and energy density, at least above the (unknown) electron injection energy. This means that above injection the overall electron momentum distribution must have equal form to that of the nuclear particles except for radiative losses. The synchrotron observations then yield three quantities: (i) the radio synchrotron spectrum will be steeper than in the test particle approximation; interpreting this in terms of nonlinear modification determines then the ion injection rate (ii) the requirement that these radio electrons have energies ≤ 1 GeV gives the value of B_{eff} (iii) the electron density amplitude from the magnitude of the synchrotron emission determines the electron:proton ratio. The actual average nuclear CR density in the SNR is reduced from the calculated spherically symmetric ion amplitude by the ratio f_{re} of the area of efficient injection to the total SNR surface area (Renormalization)[45].

4. SN 1006

In the radio and in nonthermal X-rays SN 1006 has a dipolar structure [20,47]. This is consistent with ion injection theory, as described above and with a diameter of 0.5° it should be an extended TeV source as well, allowing a test of the γ-ray morphology. From astronomical measurements at radio and X-ray wavelengths the distance is about 1.8 kpc, and the expansion velocity amounts to 3000 km/sec. A rather uncertain astronomical parameter is the density n of the ambient Interstellar Medium (ISM). In the following we use a value $n = 0.3\ cm^{-3}$ which is suggested by X-ray measurements. However, the density could be as low as $n = 0.1\ cm^{-3}$ since SN 1006 is located relatively far above the Galactic Plane. This also suggests a standard interstellar magnetic field of several μG, rather uniform on the scale of the SNR. However, as emphasized below, the effective field is expected to be substantially higher than this.

4.1. Model calculations for SN 1006

I shall now paraphrase the detailed model calculations [46] that are based on the theory discussed before. The overall hydrodynamic quantities are given in Fig. 5b. From a simultaneous fit of the observed SNR radius and expansion speed at the known age of the system of almost 1000 years the total mechanical explosion energy must be chosen as $E_{SN} = 3\ 10^{51}$; E_{SN} is somewhat high compared to the canonical 10^{51} erg. The total shock compression ratio is substantially above the

adiabatic value for a strong shock. The spherically symmetric calculation gives a total CR energy $E_c \approx 0.6 E_{SN}$ at late times. However, the renormalization factor is 0.2 [45]. This results in a fraction of about 10 % in nuclear CR energy at the late Sedov phase, when the source particles are expected to be released into the ISM.

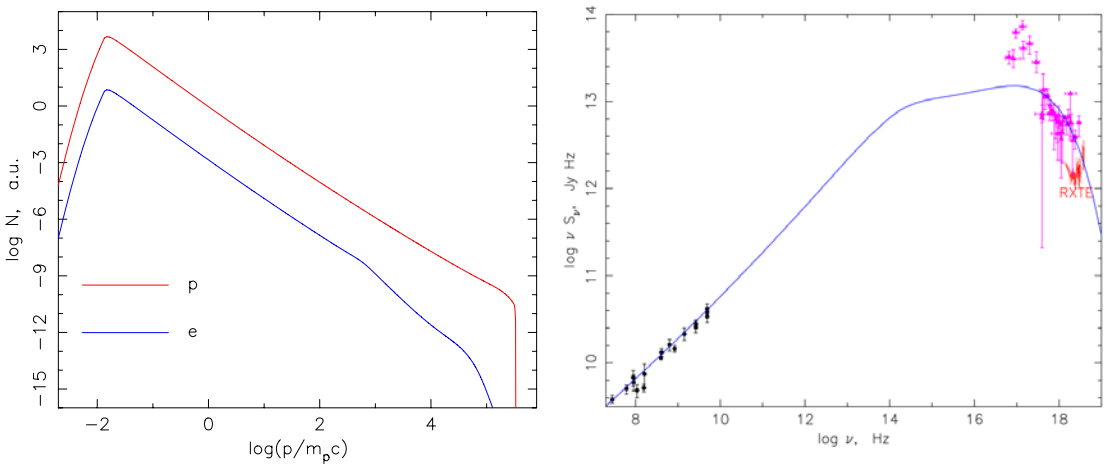

Fig. 6. Volume-integrated particle distributions N and synchrotron spectra νS_ν for accelerated protons (p) and electrons (e) in SN 1006 [46]. The observational data are the same as in Fig. 3a.

The spatially integrated spectra of CR electrons and nuclei(Fig. 6a) harden towards the cutoff, except for electron cooling. The high effective internal field $B_{eff} \approx 120$ μG is determined from the spectral slope of the radio synchrotron spectrum in Fig. 6b which also fixes the injection rate to about 10^{-4} times the flux of incoming particles. The flattening of the high frequency synchrotron spectrum also allows a smooth connection below the thermal X-rays to the hard X-ray data points. All this implies a somewhat low predicted electron:proton ratio in the overall number of accelerated particles of about $2 \cdot 10^{-3}$ for this source, compared to the canonical interstellar value of 10^{-2}.

The predicted contributions to the differential γ-ray energy spectrum, integrated over the SNR volume, are shown in Fig. 7a and the radial γ-ray brightness at 3 TeV is exhibited in Fig. 7b. For the assumed ISM density n the IC contribution from CR electrons is about one order of magnitude below the hadronic contribution due to π^0-decay, which in turn is still below the EGRET upper limits. As consequence of synchrotron cooling, the IC emission spectrum has an almost identical form to the hadronic γ-ray spectrum from several GeV up to the cutoff. This makes attempts for a distiction of spectral slopes very difficult except at very low and very high energies.

It is in this context important to note that the π^0-decay γ-ray flux scales like n^2 to lowest order, although the strong nonlinearity of the system makes this

scaling only a rough first approximation. Decreasing the external density by a factor of 2 will therefore diminish the hadronic γ-ray flux by a factor of about 4. At the same time the electron:proton ratio will increase, whereas the derived total energy E_{SN} will decrease. An external density which is lower than $n = 0.3\ cm^{-3}$ may explain the fact that the individual H.E.S.S. telescopes in Namibia have not been able to detect SN 1006 at the level suggested by the CANGAROO results.

Fig. 3b in fact indicates an IC spectrum similar to the one used to explain the more recent data points given by the CANGAROO II telescope [36]. Such a spectrum is the result of a scenario that neglects acceleration of nuclear particles and assumes an average internal field of about 10 μG, appropriate for an MHD-compressed ISM magnetic field of several μG. The form of this spectrum is different from both the hadronic and the cooled IC spectra above a few GeV. Nevertheless, a well-defined observational γ-ray spectrum is required to distinguish this scenario from the solid line spectra calculated from the nonlinear theory if the fluxes are comparable.

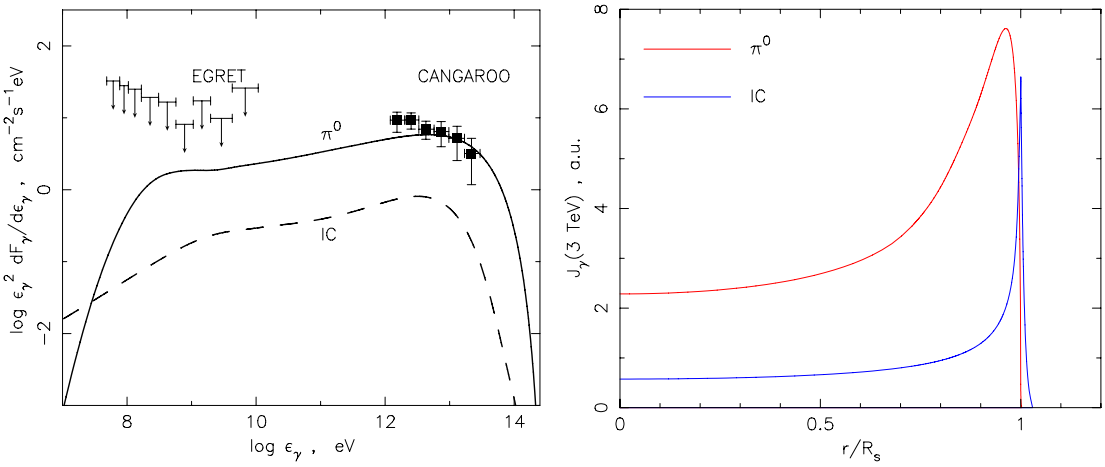

Fig. 7. Predicted differential energy spectrum of π^0-decay and IC emission (left panel), and γ-ray brightness (at 3 TeV) as functions of radius r in units of the shock radius R_s (right panel), for SN 1006 for an ambient density $n = 0.3\ cm^{-3}$. Upper limits from EGRET and the reported CANGAROO fluxes are indicated [46].

The picture becomes richer when we consider the morphology as well, for instance the radial dependence in the neighborhood of the dipole axis (Fig. 7b, for a γ-ray energy of 3 TeV). Here the IC emission is concentrated into an extremely small scale $l_e \sim 10^{-2} R_s$ near the shock at $r = R_s$ as a consequence of synchrotron cooling of the generating $\sim$ 100 TeV electrons. Also the hadronic component is fairly strongly confined to a narrow shell, since the thermal gas is concentrated there. The emission morphology for a low-field scenario (not shown here) would be considerably more extended, only exhibiting the large-scale adiabatic expansion

losses in the interior. In summary, the γ-ray emission is expected to show a dipolar spatial morphology [48], similar to that of the synchrotron emission.

An important observational result has been recently been found in Chandra observations at X-ray energies in the 1 to 10 keV region [47,49] (Fig. 8a).

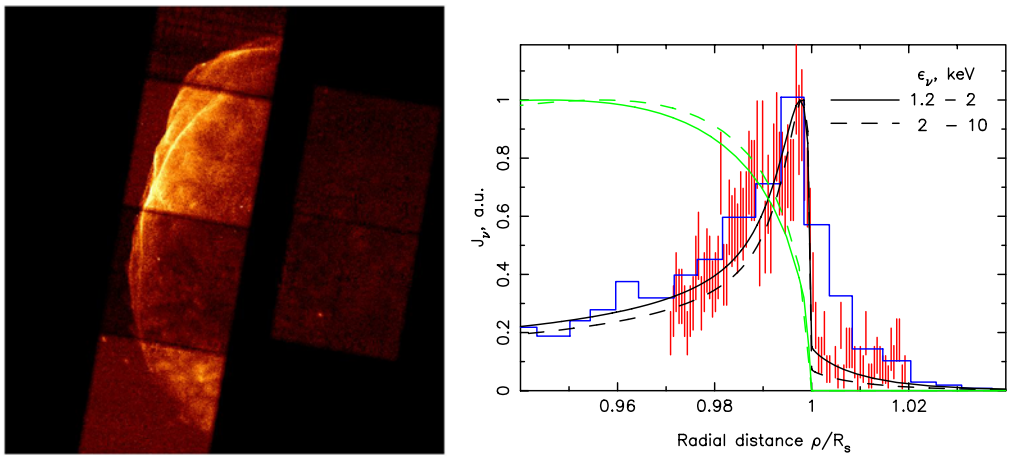

Fig. 8. Northeast limb of SN 1006, as seen by Chandra between 0.5 and 2 keV [47] (left), and projected X-ray brightness of the most narrow structure, compared with the theoretical prediction [50] (right). Vertical dashes are from [49], histogram from [47]. The thin curves correspond to the low-field scenario in Fig. 3a.

They demonstrate very narrow spatial X-ray emission structures, on a scale of $10^{-2}R_s$, confirming the magnetic field amplification made possible by a nonthermal particle population dominated by nuclear particles [46,50]. In contrast, the low-field scenario clearly fails when compared to the observations (Fig. 8b).

As a corollary, the electron population cannot create the strong field fluctuations and the required high effective field by itself [50]. This means that the dominant accelerating nuclear component is not only possible experimentally as well as theoretically: it is also necessary.

5. Cassiopeia A

This SN type Ib, whose progenitor was probably a massive Wolf-Rayet star, is on the other end of the scale of Supernovae when compared with SN 1006. Such massive progenitor stars modify the circumstellar medium through substantial mass-loss during several successive stellar wind phases: the fast rarefied Blue Supergiant wind during the main sequence phase turns into a massive but slow Red Supergiant (RSG) wind at a late stage, to be subsequently compressed from inside by yet another fast wind, now from the emerging Wolf-Rayet star, until this star finally collapses as Supernova. The turbulent compressed shell of the RSG material has a high gas density of about 10 cm^{-3} owing to radiative cooling and

is identified with the so-called bright ring in Cas A [51], see Fig. 2. According to this picture, the SNR's leading shock has already reached the unperturbed RSG wind region.

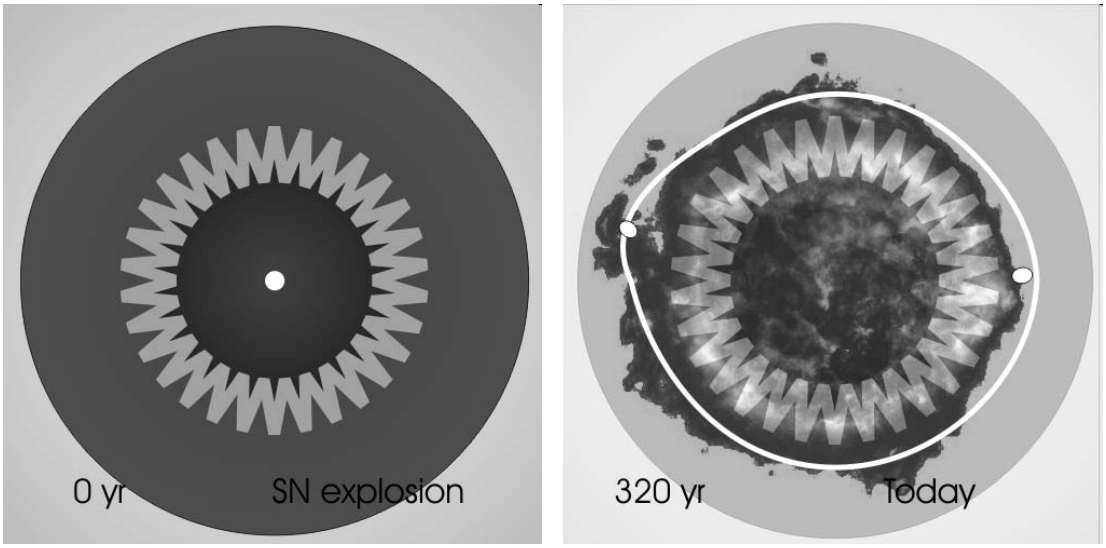

Fig. 9. Schematic of Cas A's circumstellar environment at different stages of evolution. Left panel: At explosion the turbulent shell is bordered by the interior Wolf-Rayet wind bubble and the exterior Red Supergiant wind region. Right panel: Today's SNR shock and clumpy ejecta (white spots) beyond the shocked shell and part of the Red Supergiant wind region, superposed on radio image of Fig. 2. (Courtesy G. Pühlhofer).

The HEGRA telescope system observed Cas A for 232 hours, the longest pointing used in γ-ray astronomy until now, and finally detected the source at 3.3 percent of the Crab level [52]. The acceleration model summarized here [53] basically follows the picture described above and assumes a Parker spiral type mean circumstellar magnetic field topology. The initial configuration before explosion is schematically shown in Fig. 9a, while Fig. 9b pictures the situation of today.

Given the synchrotron spectrum, the evolution of this complex system containing the turbulent wind shell allows a consistent description of the SNR dynamics with a total mechanical energy $E_{SN} = 4 \cdot 10^{50}$ erg, a present shock speed $V_s = 2000$ km/sec, and a very large downstream effective field $B_{eff} = 1$ mG in the shell. Even though the available synchtrotron observations are seperated by 30 years, about 10 % of the remnant's age, a good fit to the hardening radio spectrum is possible, followed by a synchrotron cooling range in the infrared to X-ray range, ending in a cutoff at nonthermal hard X-rays (Fig. 10a). Also the observed temporal decrease of the synchrotron emission is consistent with the picture of shock propagation into an expanding wind region of decreasing gas

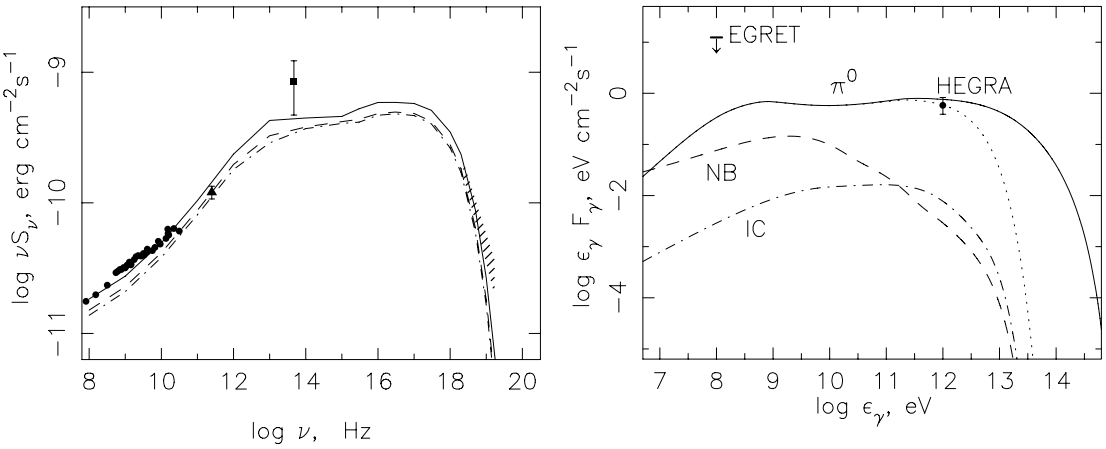

Fig. 10. Calculated synchrotron spectra at epochs 1970 (*solid curve), 2002 (dashed curve) and 2022 (dashed-dotted curve), respectively, together with observational data over a comparable time span (left panel). The right panel shows the predicted integral γ-ray energy spectrum: Nonthermal Bremsstrahlung (NB, dashed line) and IC emission (dash-dotted line), together with dominant π^0-decay emission (solid line) are far below the EGRET upper limit, but agree with the HEGRA flux at 1 TeV. The dotted line indicates a possibly lowered proton cutoff as a result of particle escape from the SNR [53].*

density.

The predicted differential γ-ray energy spectrum is shown in Fig. 10b. As a consequence of the high values of gas density and effective magnetic field strength, it is completely dominated by hadronic γ-rays from π^0-decay which are still two orders of magnitude below the EGRET upper limit. The hadronic flux has been renormalized by a factor $f_{re} = 1/6$ [45]. This prediction reasonably agrees with the observed γ-ray flux value around 1 TeV. The predicted IC and nonthermal Bremsstrahlung fluxes are very low. We therefore conclude that Cas A is a hadronic γ-ray source. The predicted proton spectrum reaches the knee region. Even if escape of CR nuclei from the weakening shock is likely to set in already at this low age, Cas A could be considered as a member of the hypothetical CR source population of Galactic SNRs.

6. A few personal theses

I want to summarize this talk in a few personal theses. I call them personal because they may not reflect the position of the two other speakers. On the other hand, the conclusions are based on the joint efforts of E.G. Berezhko, L.T. Ksenofontov, G. Pühlhofer and myself, and to this extent they are not only my own conclusions:

- The astrophysical processes of CR origin up to the knee are basically un-

derstood. The sources are the Galactic SNRs. This concerns 99.9 percent of the total energy density in CRs.

- Gamma-ray observations for SNRs are critical since only γ-rays have individual energies comparable to those of the generating charged particles. Currently experimental results are still scarce.

- The nonthermal synchrotron properties are an indispensible multi-wavelength aspect of SNRs. This concerns both the morphology and the spectrum.

- On account of the hard SNR spectra, the most appropriate instruments at γ-ray energies are large ground-based detectors like CANGAROO III, H.E.S.S., MAGIC and VERITAS. They will play a decisive role for the determination of the morphologies as well as the spectra of individual objects. They are needed to increase the detection statistics of SNRs.

- The most important global astronomical test is the detection and spectral decomposition of the "diffuse" TeV γ-ray background in the Galactic Plane to which the entire Galactic SNR population contributes.

7. Acknowledgements

I am grateful to F.A. Aharonian, E.G. Berezhko, G. Heinzelmann, L.T. Ksenofontov, G. Pühlhofer, and O. Reimer for discussions on various aspects of this manuscript.

8. References

1. Baade W., Zwicky F. 1934, Proc. Nat. Acad. Sci. USA, 20, 259
2. Dorfi, E. 1991, A&A, 251, 597
3. Drury L. O'C., Aharonian F.A., Völk H.J. 1994, A&A, 287, 959
4. Naito T., Takahara F. 1994, J. Phys. G, 20, 477
5. Gaisser T.K., Protheroe R.J., Stanev T. 1998, ApJ, 492, 219
6. Berezhko E.G., Völk, H. J. 1997, Astropart. Phys., 7, 183
7. Berezhko, E.G., Völk H.J. 2000, A&A, 357, 283
8. Berezhko E.G., Yelshin V.K., Ksenofontov L.T. 1994, Astropart. Phys., 2, 215
9. Berezhko E.G., Ksenofontov L.T., Yelshin V.K. 1995, Nucl. Phys. B (Proc.Suppl.), 39A, 171
10. Jones F.C., Ellison D.C. 1991, Space Sci. Rev. 58, 259
11. Baring M.G., Ellison D.C., Reynolds S.P. et al. 1999, ApJ, 513, 311
12. Esposito J.A., Hunter S.D., Kanbach G. et al. 1996, ApJ, 461, 820
13. Buckley J.H., Akerlof C.W., Carter-Lewis D.A. et al. 1998, A&A, 329, 639
14. Heß M. (HEGRA Collaboration) 1997, Proc. 25th ICRC (Durban), 3, 229
15. Tanimori T., Hayami Y., Kamei S. et al. 1998, ApJ, 497, L25

16. Völk H.J. 1997, in: de Jager O.C. (ed.) Towards a Major Atmospheric Cherenkov Detector – V, Kruger Park, p. 87 ff.
17. Brazier K.T.S., Kanbach G., Carraminana A. et al. 1996, MNRAS, 281, 1033
18. Keohane J.W., Petre R., Gotthelf E.V. et al. 1997, ApJ, 484, 350
19. Sturner S.J., Keohane J.W., Reimer O. 2003, in: "High Energy Studies of Supernova Remnants and Neutron Stars", 34th COSPAR Symp., Houston 2002, Eds. W.Hermsen and W. Becker, Advances in Space Resarch, in press
20. Koyama, K., Petre, R., Gotthelf, E.V. et al. 1995, Nature, 378, 255
21. Allen G.E., Gotthelf E.V. & Petre R. 1999, Proc. 26the ICRC (Salt Lake City), 3, 480
22. Reynolds S.P. 1996, ApJ, 459 , L13
23. Hamilton A.J.S., Sarazin C.L. & Szymkowiak A.E. 1986, ApJ, 300, 698
24. Koyama K., Kinugasa K., Matsuzaki K. et al. 1007, PASJ, 49, L7
25. Slane P., Gaensler B.M., Dame T.M. et al. 1999, ApJ, 525, 357
26. Allen G.E., Keohane J.W., Gotthelf E.V. 1997, ApJ, 487, L97
27. Pohl M. 1996, A&A, 307, L57
28. Mastichiadis A., de Jager O.C. 1996, A&A, 311, L5
29. Muraishi H., Tanimori T., Yanagita S. et al. 2000, A&A, 354, L57
30. Aharonian F.A., Atoyan A.M. 1999, A&A, 351,330
31. Weekes T.C. 2001, in: High Energy Gamma-Ray Astronomy (ed. F.A. Aharonian, H.J. Völk), AIP Conf. Proc. 558, Melville, New York, p. 15 ff.
32. Enomoto R., Tanimori T., Naito T. et al. 2002, Nature, 416, 823
33. Reimer O., Pohl M. 2002, A&A, 390, L43
34. Butt Y.M., Torres D.F., Romero G.E. et al. 2002, Nature, 418, 499
35. Uchiyama Y., Aharonian F.A., Takahashi T. 2003, A&A, 400, 567
36. Tanimori T., Naito T., Yoshida T. et al. 2001, Proc. 27th ICRC (Hamburg), 6, 2465
37. Drury L.O'C. 1983, Rep. Prog. Phys., 46, 973
38. Völk, H. J. 1984, in: High Energy Astrophysics, ed. J. Tran Thanh Van, Editions Frontieres, Gif sur Yvette
39. Blandford R.D., Eichler D. 1987, Phys.Rept., 154, 1
40. Berezhko E.G., Krymsky G.F. 1988, Soviet Phys.-Uspekhi., 12, 155
41. Malkov M.A., Drury L.O'C. 2001, Rep. Prog. Phys., 64, 429
42. McKenzie, J.F., Völk, H.J. 1982, A&A, 116, 191
43. Lucek S. G., Bell A. R. 2000, MNRAS, 314, 65
44. Bell A. R., Lucek S. G. 2001, MNRAS, 327, 433
45. Völk H.J., Berezhko E.G., Ksenofontov L.T. 2003, A&A, 409, 563
46. Berezhko E.G., Ksenofontov L.T., Völk H.J. 2002, A&A, 395, 943
47. Long K.S., Reynolds S.P., Raymond J.C. et al. 2003, ApJ, 586, 1162
48. Konopelko A., Lucarelli F., Lampeitl H., Hofmann W. 2002, J. Phys.G, 28, 2755

49. Bamba A., Yamazaki R., Ueno M., Koyama K. 2003, ApJ, 589, 827
50. Berezhko E.G., Ksenofontov L.T., Völk H.J. 2003, to appear in A&A Lett. (astro-ph/0310862)
51. Borkowsky K.J., Szymkowiak A.E., Blondin J.M. et al. 1996, ApJ, 466, 866
52. Aharonian F.A., Akhperjanian A., Barrio J. et al. 2001, A&A, 370, 112
53. Berezhko E.G., Pühlhofer G., Völk H.J. 2003, A&A, 400, 971